



RESEARCH LETTER

10.1002/2016GL071661

Key Points:

- Subtropical South Pacific is one of the Earth's major heat accumulators and accounts for up to a quarter of the global ocean heat increase
- Indirect and direct estimates based on satellite and in situ data show significant local heat accumulation below 2000 m depth
- Heat accumulation is due to a decade-long intensification of wind-driven convergence possibly linked to persistent La Niña-like conditions

Supporting Information:

- Supporting Information S1

Correspondence to:

D. L. Volkov,
denis.volkov@noaa.gov

Citation:

Volkov, D. L., S.-K. Lee, F. W. Landerer, and R. Lumpkin (2017), Decade-long deep-ocean warming detected in the subtropical South Pacific, *Geophys. Res. Lett.*, 44, 927–936, doi:10.1002/2016GL071661.

Received 20 OCT 2016

Accepted 5 DEC 2016

Accepted article online 9 DEC 2016

Published online 18 JAN 2017

Decade-long deep-ocean warming detected in the subtropical South Pacific

Denis L. Volkov^{1,2} , Sang-Ki Lee² , Felix W. Landerer³ , and Rick Lumpkin² 

¹Cooperative Institute for Marine and Atmospheric Studies, University of Miami, Miami, Florida, USA, ²Atlantic Oceanographic and Meteorological Laboratory, National Oceanic and Atmospheric Administration, Miami, Florida, USA, ³Jet Propulsion Laboratory, California Institute of Technology, Pasadena, California, USA

Abstract The persistent energy imbalance at the top of the atmosphere, inferred from satellite measurements, indicates that the Earth's climate system continues to accumulate excess heat. As only sparse and irregular measurements of ocean heat below 2000 m depth exist, one of the most challenging questions in global climate change studies is whether the excess heat has already penetrated into the deep ocean. Here we perform a comprehensive analysis of satellite and in situ measurements to report that a significant deep-ocean warming occurred in the subtropical South Pacific Ocean over the past decade (2005–2014). The local accumulation of heat accounted for up to a quarter of the global ocean heat increase, with directly and indirectly inferred deep ocean (below 2000 m) contribution of 2.4 ± 1.4 and $6.1\text{--}10.1 \pm 4.4\%$, respectively. We further demonstrate that this heat accumulation is consistent with a decade-long intensification of the subtropical convergence, possibly linked to the persistent La Niña-like state.

1. Introduction

The ocean, covering 71% of the Earth's surface, serves as the major energy reservoir [Levitus *et al.*, 2005], and the well-documented global mean sea level rise is one of the most certain indicators of global warming [Intergovernmental Panel on Climate Change (IPCC), 2013; Church and White, 2011]. Sea level rises due to the thermal expansion of the entire water column (from ocean warming) and the freshwater input from melting glaciers and ice sheets (mainly in Greenland and Antarctica). As the ocean is warming and its volume is expanding (as evidenced by both satellite and in situ measurements), the question of heat sequestration at depth has attracted much attention [Trenberth and Fasullo, 2010; Purkey and Johnson, 2010; Hansen *et al.*, 2011; Loeb *et al.*, 2012; Abraham *et al.*, 2013; Balmaseda *et al.*, 2013; Johnson and Lyman, 2014; Cazenave *et al.*, 2014; Llovel *et al.*, 2014; Chen and Tung, 2014; Purkey *et al.*, 2014; Desbruyères *et al.*, 2016].

Combination of the present-day satellite and in situ observing systems has a potential to provide a more complete view on the horizontal and vertical distributions of heat in the ocean. Sea level has been continuously measured by altimetry satellites since 1992 with a nearly global coverage and high accuracy. Since the early 2000s, Argo floats (nearly global coverage achieved in 2005) and Gravity Recovery and Climate Experiment (GRACE) satellites (launched in 2002) have provided measurements of ocean temperature and salinity in the upper 2000 m and estimates of ocean mass changes, respectively. The difference between the total sea level (observed by altimetry) and the mass-related sea level (observed by GRACE) gives the steric (due to changes in seawater density) sea level variability, which is mostly a function of the full-depth heat content [Jayne *et al.*, 2003]. The deep-ocean (below 2000 m) contribution can be inferred indirectly as the difference between the satellite-based (altimetry minus GRACE) and Argo-based steric sea level [Willis *et al.*, 2008; Llovel *et al.*, 2014]. The most recent synthesis of satellite altimetry, GRACE, and Argo measurements showed that no significant deep-ocean warming occurred on the global scale during the 2005–2013 period [Llovel *et al.*, 2014; Dieng *et al.*, 2015]. On the other hand, several studies based on repeat hydrography sections (mostly during the pre-Argo era) have reported a statistically significant deep-ocean warming from 1990s to 2000s, mainly concentrated in the Southern Ocean [Abraham *et al.*, 2013; Purkey and Johnson, 2010, 2012; Desbruyères *et al.*, 2016]. Because the existing observing systems are subject to uncertainties and temperature measurements below 2000 m are rather sparse and irregular, the topic of deep-ocean warming is still controversial and requires further research.

The deep-ocean warming can initiate and advance in the regions where the air-sea interactions and ocean internal dynamics favor transfer of heat from the surface to the deeper waters. It is important to identify such

regions, preferably by using as many independent observing systems as possible, and to understand the associated dynamics. Carrying out a comprehensive analysis of satellite and in situ measurements, and atmospheric re-analyses, this study reports on deep-ocean warming signatures observed in the subtropical South Pacific during the past decade of 2005–2014 and shows that this warming is consistent with a decade-long intensification of the Southern Hemispheric westerly and trade winds and associated subtropical convergence, possibly linked to the persistent La Niña-like conditions.

2. Data and Methodology

For the total sea level, we used the monthly satellite altimetry maps of sea surface height (SSH) from January 2002 to December 2015 produced by Ssalto/Duacs and distributed by Aviso (www.aviso.oceanobs.com). For the mass component of SSH change, SSH_{Mass} , we used the monthly GRACE ocean grids (www.grace.jpl.nasa.gov), derived from the JPL-RL05M mass concentration blocks or “mascons” (JPL-Mascons or MSC) and the RL05 spherical harmonics from CSR (Center for Space Research, University of Texas), GFZ (German GeoForschungsZentrum), and JPL (Jet Propulsion Laboratory). In addition to standard GRACE corrections [Cheng and Tapley, 2004; Swenson et al., 2007; Geruo et al., 2013], we applied a correction for the Earth’s pole tide effect [Wahr et al., 2015] that considerably reduced discrepancies in regional trends among the GRACE products (Text S1 in the supporting information).

The monthly estimates of the upper 2000 m steric sea level (SSL_{2000}) in 2004–2015 were obtained from the gridded temperature and salinity profiles provided by the Scripps Institution of Oceanography (SIO) [Roemmich and Gilson, 2009] and the Japan Agency for Marine–Earth Science and Technology (JAMSTEC) [Hosoda et al., 2008] (<http://www.argo.ucsd.edu>). The SIO data are based on Argo float measurements only, while the JAMSTEC data combine additional in situ measurements, such as CTD (conductivity-temperature-depth), XBT (expendable bathythermographs), and moorings.

The total SSH is regarded here as the sum of SSH_{Mass} , SSL_{2000} , and the deep (below 2000 m) steric sea level, SSL_{Deep} (i.e., $SSH = SSH_{\text{Mass}} + SSL_{2000} + SSL_{\text{Deep}}$). While the first three components are measured by altimetry, GRACE, and (mainly) Argo floats, respectively, SSL_{Deep} is estimated as the residual.

The indirect estimates of the deep-ocean contribution to the regional sea level rise were validated against the effect of temperature differences between the two occupations of section P16 (Figure 1) in January–February 2005 and March–May 2014. The hydrography data are provided by Climate Variability and Predictability and Carbon Hydrographic Data Office (<http://cchdo.ucsd.edu>).

The net surface heat flux estimates were obtained from the ERA-Interim [Dee et al., 2011], National Centers for Environmental Prediction 2 (NCEP-2) [Kanamitsu et al., 2002], and Modern-Era Retrospective Analysis for Research and Applications (MERRA) [Rienecker et al., 2011] re-analysis products. Ekman pumping was computed by using ERA-Interim wind stress data. A monthly climatology computed as the multiyear averages for each calendar month over 2005–2014 was removed from all estimates presented in this study.

The uncertainties for each observing system (Table 1) are based on comparisons with tide gauges (for SSH), ocean models and bottom pressure recorders (for SSH_{Mass}) [Chambers and Bonin, 2012; Mazloff and Boening, 2016], and on temperature and salinity errors at each grid point contained in JAMSTEC data (for SSL_{2000}). The linear trend uncertainties are the 95% confidence intervals accounting for the slope in the data and random measurement errors (fourth column of Table 1). A more detailed discussion of data products used and uncertainty estimates can be found in Text S1 [Ablain et al., 2009, 2015; Le Traon et al., 1998; Johnson and Chambers, 2013; Menemenlis et al., 2008; Peltier, 2004].

3. Results

3.1. The Earth’s Major Heat Accumulators

Subtracting SSH_{Mass} from SSH yields the steric sea level over the entire water column (SSL). It is reasonable to look for the signs of deep-ocean warming in the regions of heat accumulation, as revealed by the satellite-based SSL trend over 2005–2014, which displays striking regional differences of $\pm 15\text{--}20 \text{ mm yr}^{-1}$ (Figure 1a). While the global mean SSL rose at a rate of $1.3 \pm 0.4 \text{ mm yr}^{-1}$ (Text S2), the largest increase of SSL occurred in the Indian and South Pacific oceans. An abrupt increase of the upper 700 m heat content in the Indian Ocean in

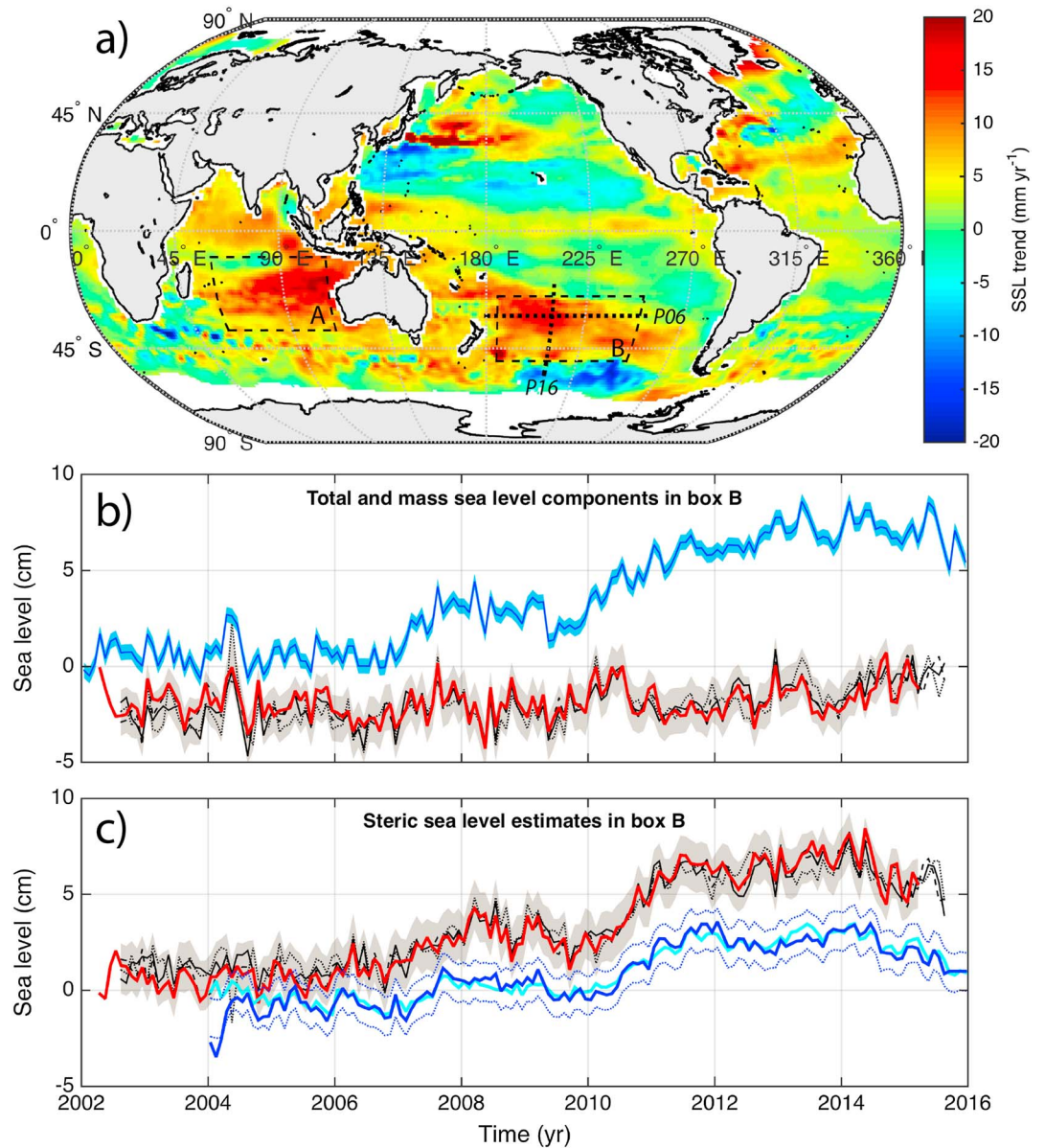


Figure 1. (a) Satellite-based (altimetry minus GRACE-CSR) steric sea level trend over 2005–2014. The dashed rectangles A and B outline the regions considered in this study. The dotted lines across box B denote P16 and P06 repeat hydrographic sections. (b) SSH from satellite altimetry (blue), SSH_{Mass} from GRACE Mascons (red), CSR (solid black), GFZ (dotted black), and JPL (dashed black) products. (c) SSL estimates computed by subtracting GRACE Mascons (red), CSR (solid black), GFZ (dotted black), and JPL (dashed black) data from the altimetry record and the upper 2000 m steric sea level computed from SIO (cyan) and JAMSTEC (blue) products. Figures 1b and 1c refer to box B. The shading (for altimetry, GRACE, and the difference between them) and dotted curves (for the upper 2000 m steric sea level) indicate measurement uncertainties (fourth column of Table 1). The time series shown are offset for clarity.

2000s has been attributed to an enhanced heat transport from the equatorial western Pacific owing to La Niña-like conditions [Lee *et al.*, 2015]. A large buildup of the upper 2000 m heat content in the South Pacific since 2006 has also been documented and attributed to wind-driven convergence [Roemmich *et al.*, 2015, 2016; Volkov *et al.*, 2015].

Boxes A in the South Indian (60–110°E, 10–38°S) and B in the South Pacific (185–250°E, 25–50°S) oceans (Figure 1a) each contributed nearly $25 \pm 5\%$ of the global mean SSL rise in 2005–2014 (Text S2). Although the two regions appear to be the Earth’s major heat accumulators, they differed from each other in two important aspects: (i) unlike the South Pacific, the SSL rise in the South Indian Ocean was to a large extent

Table 1. Sea Level Trends Over the 2005–2014 Time Interval in Box B and Their Uncertainties for Different Depth Intervals and Data Products^a

Depth Interval (m)	Parameter	Observational Products	Uncertainty (mm)	Sea Level Trend 2005–2014 (mm yr ⁻¹)
0 to bottom	SSH	ALT (AVISO)	4	8.3 ± 0.8
		SSH _{Mass}	MSC (GRACE)	12
	SSL	CSR (GRACE)		1.6 ± 1.1
		GFZ (GRACE)		1.9 ± 1.2
		JPL (GRACE)		1.3 ± 1.1
0–2000	SSL ₂₀₀₀	ALT-MSC	13	7.4 ± 1.3
		ALT-CSR		6.7 ± 1.3
		ALT-GFZ		6.4 ± 1.3
		ALT-JPL		7.0 ± 1.3
		SIO	10	4.5 ± 0.9
		JAMSTEC		4.4 ± 1.0
		2000 to bottom	SSL _{Deep}	ALT-MSC-SIO
ALT-MSC-JAMSTEC				3.0 ± 1.3
ALT-CSR-SIO				2.2 ± 1.3
ALT-CSR-JAMSTEC				2.3 ± 1.3
ALT-GFZ-SIO				1.8 ± 1.4
ALT-GFZ-JAMSTEC				1.9 ± 1.4
ALT-JPL-SIO				2.4 ± 1.3
ALT-JPL-JAMSTEC				2.5 ± 1.3
Average				2.4 ± 1.3
Temperature at P16 line				0.7 ± 0.4

^aSee section 2 and Text S1 for details: altimetry (ALT); GRACE Mascons (MSC), CSR, GFZ, and JPL; and Hydrography (SIO/JAMSTEC/P16).

halosteric (due to salinity changes) [Llovel and Lee, 2015], and (ii) warming in box A was limited to the upper 1000 m, while in box B, significant warming also occurred in the 1000–2000 m depth interval (Text S3 and Figure S3 in the supporting information). This indicates that deep-ocean warming is more likely to have occurred in the South Pacific, and therefore, the following analysis is focused on box B.

3.2. Indirect Estimate of Deep-Ocean Warming

Box B is situated in a relatively quiescent part of the South Pacific subtropical gyre bordered by the eddy-rich Antarctic Circumpolar Current (ACC) to the south. Heat accumulation in box B is investigated in terms of SSL. Sea level trends, estimated from different data products, are presented in Table 1. The time series of SSH averaged over box B shows that sea level was rather stable in 2002–2006 but started to increase at a rate of 8.3 ± 0.8 mm yr⁻¹ during 2005–2014, reaching a maximum in 2013 (Figure 1b). The local change in ocean mass made a minor contribution to this rate. Our estimates show that while all four GRACE products agree on the global mean SSH_{Mass} change of about 2.0 ± 0.2 mm yr⁻¹ (similar to Llovel *et al.* [2014]), their local trends have larger uncertainties (Figure 1b and Table 1).

The estimated rates of SSL rise in box B (Figure 1c) range from 6.4 ± 1.3 mm yr⁻¹ to 7.4 ± 1.3 mm yr⁻¹ (Table 1). During the same period, the Argo-based SSL₂₀₀₀ rose at a smaller rate. The two in situ products agree with each other very well, showing similar trends of about 4.5 ± 1.0 mm yr⁻¹ (Figure 1c and Table 1). The estimated rate of SSL₂₀₀₀ rise is equivalent to the vertically averaged upper-ocean warming of about 0.15°C/decade in box B. The halosteric contribution to the decadal trend of SSL₂₀₀₀ was negligible (<1%).

The vertical profile of the decadal temperature trend in the South Pacific, based on JAMSTEC data, demonstrates a consistent warming over the entire upper 2000 m water column north of about 50°S (Figure 2a). The maximum warming in excess of 1°C occurred around 35°S and between 100 and 400 m depth; between the 1000 and 2000 m depth within box B, water warmed by up to 0.1°C. This warming in the upper 2000 m is associated with a southward movement of isotherms near the surface and a deepening of isotherms over the entire water column, in particular between 30°S and 50°S (contours in Figure 2a). At the same time, isotherms moved northward in the ACC south of 50°S, causing a cooling trend observed over the entire upper 2000 m of the water column. The decadal salinity trend is discussed in Text S4.

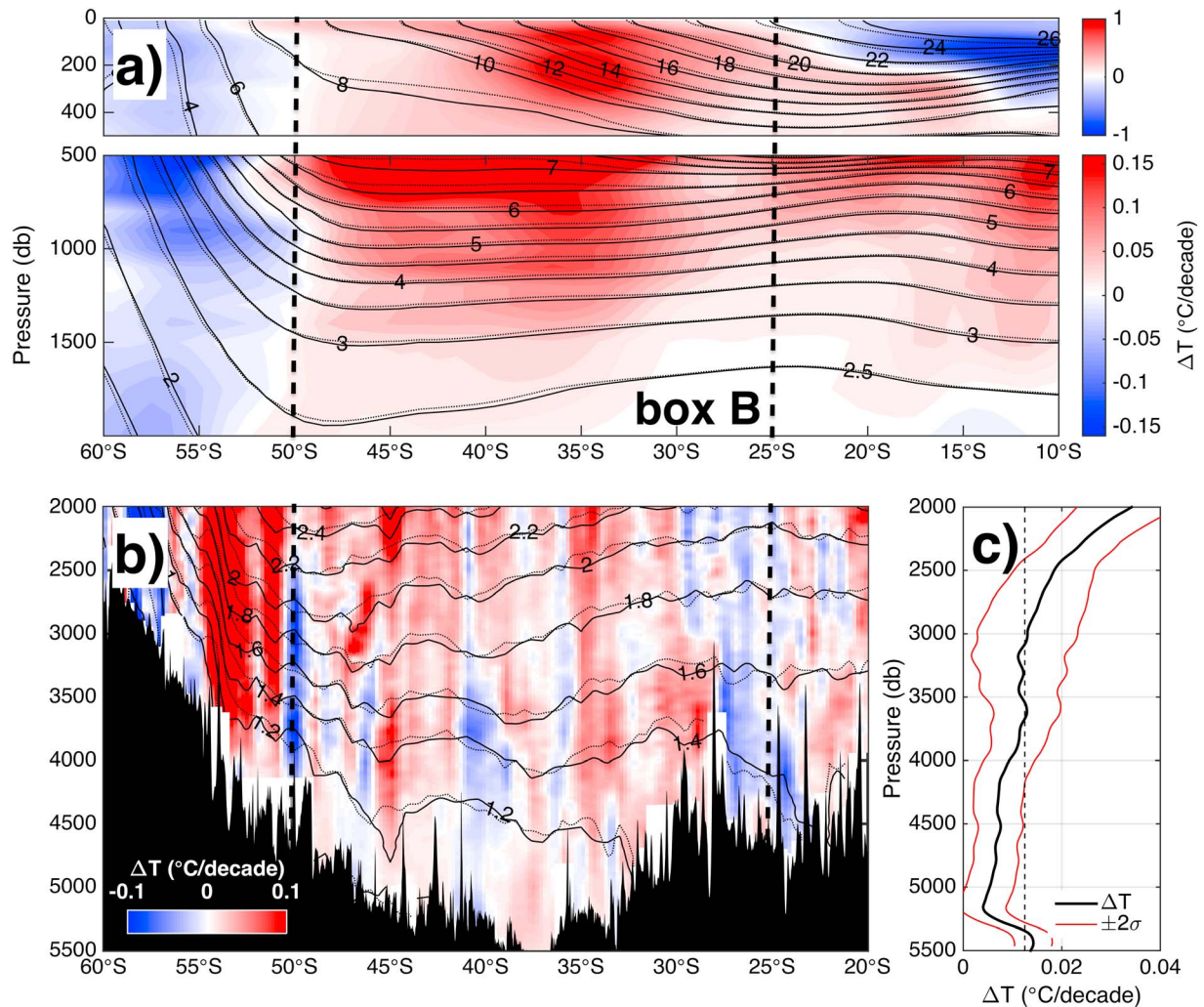


Figure 2. (a) Decadal (2005–2014) trend of the zonally averaged temperature between 185°E and 250°E from JAMSTEC data. The dotted (solid) contours show the isotherms for the first (last) months of the linear trend, respectively. (b) Difference between the temperature profiles obtained during the P16 occupations in March–May 2014 and in January–February 2005 translated into a change in °C/decade. The dotted and solid contours show the isotherms for the P16 occupations in 2005 and 2014, respectively. Note that the color scales are different for the upper 500 m, 500–2000 m, and 2000–5500 m layers. The southern and northern boundaries of box B are shown by the vertical dashed lines. (c) The vertical profile of a temperature change between the 2005 and 2014 occupations of the P16 section averaged between 25°S and 50°S (black curve) and translated into a change in °C/decade. The vertical dashed line indicates the 2000–5500 m average temperature change of 0.012°C. The red curves indicate the 95% confidence intervals (see Text S1 for details).

As suggested by the estimates based on different data products (Figure 3a and Table 1), SSL_{Deep} averaged over box B rose at rates ranging from $1.8 \pm 1.4 \text{ mm yr}^{-1}$ to $3.0 \pm 1.3 \text{ mm yr}^{-1}$. This is equivalent to a depth-averaged (between 2000 and 5500 m) temperature change from $0.032 \pm 0.024^\circ\text{C/decade}$ to $0.050 \pm 0.022^\circ\text{C/decade}$ (Text S1), assuming that the halosteric contribution at depth is negligible. The relatively wide range of values is mainly due to uncertainties in the local GRACE trends.

3.3. Direct Estimate of Deep-Ocean Warming

Box B includes three repeat hydrographic transects (P06, P15, and P16) that provide independent temperature measurements at depths below 2000 m. However, only P16 along 150°W (Figure 1a) was occupied at the beginning (January–February 2005) and near the end (March–May 2014) of the study period. Given the strong interannual variability of heat content in the region (Figure S3), it is only reasonable to consider temperature changes over approximately the same time interval as the study period (2005–2014), and therefore, here we consider only P16 transect. For comparison, because of the interannual variability, temperature

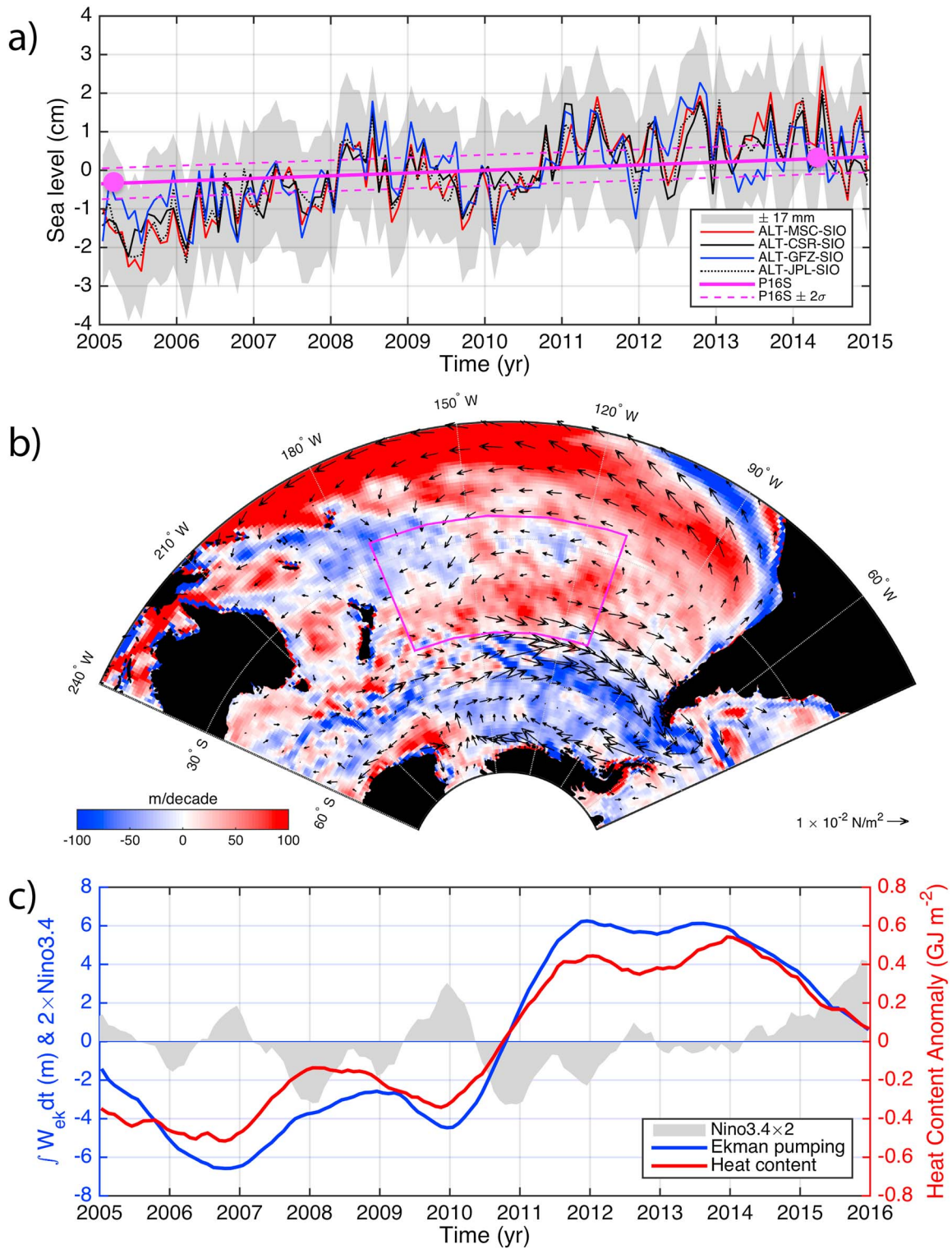


Figure 3. (a) Differences between the satellite-derived (entire water column) and in situ-derived (upper 2000 m) steric sea levels (only for SIO data), showing the indirectly derived contribution of the deep ocean (2000 m to bottom) for different GRACE products (see Table 1). The uncertainty (shaded area) is shown with respect to the ensemble averaged time series. The $0.7 \pm 0.4 \text{ mm yr}^{-1}$ sea level trend derived from temperature measurements below 2000 m along P16 transect is shown by the magenta dots. The magenta dots signify the times of P16 occupation. (b) The 2005–2014 averaged wind stress (arrows) and Ekman pumping (color; positive downward) anomalies relative to the climatological (1979–2015) mean fields. (c) Cumulative sum of the Ekman pumping anomaly (blue) and heat content anomaly (red) averaged over box B in the South Pacific. The time series are smoothed with a yearly running mean. The monthly Niño3.4 index scaled by 2 is shown by grey-shaded area.

differences between the two occupations of P06 transect (Figure 1a) in August–September 2003 and November–December 2009 are found insignificant (discussed in Text S5).

Although the deep-ocean temperature difference between the two occupations of P16 (Figure 2b) is likely biased by eddies (especially in the ACC), tides, and waves that can cause the vertical displacement of isotherms, it is noticeable that between 25°S and 50°S a significant temperature rise occurred in almost the entire water column from 2000 m to about 5500 m depth (Figure 2c). On average, the deep-ocean temperature increased by $0.012 \pm 0.007^\circ\text{C}$ (dashed line in Figure 2c), which corresponds to a sea level rise of $0.7 \pm 0.4 \text{ mm yr}^{-1}$. Within the error bars this estimate agrees with the indirect estimates, based on GRACE-CSR/GFZ/JPL data (Figure 3a and Table 1). It should be noted that the direct estimate is based only on one cross section that may not be representative of the entire box B. Nevertheless, the consistency between the indirect and direct estimates suggests that deep-ocean warming (below 2000 m) in the South Pacific in 2005–2014 is very likely robust.

3.4. Dynamical Processes Responsible for Heat Accumulation

Regional heat content varies due to changes in (i) the net surface heat flux and (ii) the advection of heat by ocean currents. Based on the ERA-Interim/NCEP-2/MERRA re-analyses, the net surface heat flux (positive into the ocean) averaged over the 2005–2014 decade and over box B ($2.3/4.1/11.0 \text{ W m}^{-2}$) was smaller than the long-term (1979–2015) climatological heat flux ($5.2/6.5/12.4 \text{ W m}^{-2}$) in all products. In a statistically stable situation, where regional heat content and sea level remain unchanged, the net surface heat flux is balanced by the advection of heat by ocean currents. If heat advection is constant, then the reduction of the net surface heat flux would result in a sea level decrease. This means that the air-sea heat exchange was not the driver of the observed heat content changes and sea level rise in box B. Apparently, heat advection was strong enough to compensate for the reduction in the net surface heat flux and led to the accumulation of heat in the entire water column and associated sea level rise in the region.

Figure 3b reveals that in 2005–2014, the South Pacific and the Pacific sector of the Southern Ocean featured very strong (relative to climatology) trade winds in the tropics and westerly winds over the ACC, during which a persistent La Niña-like condition prevailed (i.e., predominantly negative Niño3.4 index) (Figure 3c). The strongest anomalies of westerly winds reached about 1 m s^{-1} and were observed along 50°S and between 80°W and 140°W. The trade wind anomalies were even stronger, exceeding 1.5 m s^{-1} , and concentrated in the western equatorial Pacific.

Westerly winds over the ACC and easterly trade winds in the tropics drive northward and southward (near surface) Ekman transports, respectively, that converge in the subtropical South Pacific. The intensified Ekman transports in 2005–2014 apparently led to the horizontal shifts of isotherms and isohalines in the upper ocean (discussed above and in Text S4): northward in the ACC and southward in the tropics and subtropics (Figure 2a). The horizontal divergence/convergence of Ekman transports leads to a vertical velocity in the upper frictional boundary layer of the ocean (Ekman pumping). Strengthening of the wind stress curl in the subtropical South Pacific led to an intensification of downward Ekman pumping (positive downward) with a local maximum located within box B (Figure 3b). The increased convergence at the ACC Polar Front apparently resulted in an enhanced production of the lower salinity Antarctic Intermediate Water (Figure S4).

The time integral of Ekman pumping averaged over box B yields anomalies in the vertical displacement of the thermocline (Figure 3c). The observed downward shift of isotherms in 2005–2014 (Figures 2a and 2b) implies that downward Ekman pumping may have also affected the deeper layers. Interestingly, the time integral of Ekman pumping is well correlated with the upper 2000 m heat content anomaly (Figure 3c) and consistent with the observed temperature increase at depth (Figures 2b and 3a). These results support the recent findings of Roemmich *et al.* [2016] and Volkov *et al.* [2015], who suggested that the strongly intensified wind-driven convergence in the subtropical South Pacific and the associated Ekman pumping during the decade of 2005–2014 were the main mechanisms of the observed regional upper-ocean heat accumulation and sea level rise. Our findings further suggest that persistent wind forcing affected not only the upper 2000 m but also the deeper layers due the adiabatic deepening of isotherms in the entire water column. It should be noted, however, that the inferred 2005–2014 deep-ocean warming probably reflects interannual to interdecadal variations of wind forcing, rather than a persistent long-term trend.

4. Discussion and Conclusions

The combined use of altimetry, GRACE, and Argo measurements is theoretically an ideal method to indirectly derive deep steric changes below 2000 m depth. While the uncertainties associated with the observing systems are decreasing [von Schuckmann *et al.*, 2016], the indirect method has already been found useful for sea level budget studies [Llovel *et al.*, 2014; Purkey *et al.*, 2014; Dieng *et al.*, 2015]. Our results show that with respect to local trends in box B, GRACE data have the largest uncertainty and should be used with appropriate care.

Given that SSL_{2000} accounts for about a half of the SSH rise in box B (Table 1) and the residual ($3.8\text{--}3.9 \pm 1.3 \text{ mm yr}^{-1}$) is about 2 times greater than the global mean SSH_{Mass} change ($2.0 \pm 0.2 \text{ mm yr}^{-1}$), the indirectly inferred local deep-ocean warming is likely robust. The local SSH_{Mass} change due to the melting of glaciers in Greenland and Antarctica is not expected to exceed the global mean SSH_{Mass} rise [Tamisiea and Mitrovica, 2011]. If the SSH_{Mass} rise was uniform over the globe, then the residual SSL_{Deep} rise in box B would still be significant ($1.8 \pm 1.3 \text{ mm yr}^{-1}$).

Our indirect estimates of the deep-ocean contribution to the sea level rise in box B range from $1.8 \pm 1.4 \text{ mm yr}^{-1}$ to $3.0 \pm 1.3 \text{ mm yr}^{-1}$. The direct estimate of the deep-ocean temperature change along P16 transect in 2005–2014 provides more confidence in the residual calculation. The directly measured moderate warming of $0.012 \pm 0.007^\circ\text{C}$ is equivalent to a sea level rise of $0.7 \pm 0.4 \text{ mm yr}^{-1}$, which within the error bars agrees with most indirect estimates (Table 1). According to the direct and indirect estimates and assuming that the halosteric contribution is negligible, the deep-ocean in box B contributed from $2.4 \pm 1.4\%$ to $6.1\text{--}10.1 \pm 4.4\%$ of the global ocean mean SSL and heat increase, respectively (Text S2).

By realizing the potential pitfalls of the residual calculation, we note that our study is the first to report on consistency between the indirect and direct estimates of the deep-ocean warming in the subtropical South Pacific. By focusing on the regional as opposed to the global accumulation of heat (which can be independent from each other), we reconcile the recently published studies with contrasting reports on deep-ocean temperature changes based on repeat hydrography [Purkey and Johnson, 2010; Desbruyères *et al.*, 2016] and on the residual calculation for the global ocean [Llovel *et al.*, 2014; Dieng *et al.*, 2015]. We show that the directly and indirectly inferred deep-ocean warming was consistent with the upper ocean warming in 2005–2014, and likely driven (or at least favored) by persistent wind-driven convergence intrinsic to La Niña-like conditions. This suggests that the observed warming at least partially reflects an interannual to interdecadal variation.

We note, however, that given the scarcity of observations at depth, the presented mechanism is hypothetical and other mechanisms could also be relevant. The abyssal warming, for example, can be triggered by changes in buoyancy forcing in Antarctic Bottom Water formation regions [Purkey and Johnson, 2012, 2013; Masuda *et al.*, 2010]. Overall, our study highlights the importance of the implementation of the Deep-Argo array in the region and globally, which will help to reduce uncertainties in sea level and planetary energy-imbalance budgets [Johnson *et al.*, 2015].

The findings reported here indicate that the subtropical South Pacific is a region where heat can be effectively sequestered by a convergence-favorable persistent wind forcing. Therefore, the observed decade-long regional accumulation of heat at depth could potentially contribute to the documented “hiatus” in sea surface temperatures [IPCC, 2013]. However, the subtropical South Pacific began losing heat in 2014, and this tendency continued throughout 2015 (Figure 3c). At the beginning of 2014, the Pacific Ocean and the atmosphere began exhibiting features of the impending El Niño event, which by early 2016 had already expressed itself as one of the most powerful on record. Triggered by the 2014–2016 El Niño event, a weakening of westerly winds over the ACC and trade winds in the tropics has been observed; the wind stress curl and associated Ekman pumping in the subtropical South Pacific have also decreased (Figure 3c). As a motivation for continued research, it is reasonable to hypothesize that if the cooling tendency that began in 2014 in the South Pacific continues, then the heat accumulated at depth could be released into the atmosphere and the surrounding ocean with far-reaching effects on weather and climate.

Acknowledgments

This research was supported by the NASA Ocean Surface Topography Science Team program and by the base funds of NOAA-AOML. The work of F.W. Landerer was carried out at the Jet Propulsion Laboratory, California Institute of Technology, under a contract with NASA. The authors thank two anonymous reviewers and Don Chambers for their constructive comments and helpful suggestions. All data for this paper are publicly available, properly cited, and referred to in the reference list.

References

- Ablain, M., A. Cazenave, G. Valladeau, and S. Guinehut (2009), A new assessment of the error budget of global mean sea level rate estimated by satellite altimetry over 1993–2008, *Ocean Sci.*, 5, 193–201, doi:10.5194/os-5-193-2009.
- Ablain, M., *et al.* (2015), Improved sea level record over the satellite altimetry era (1993–2010) from the Climate Change Initiative project, *Ocean Sci.*, 11, 67–82, doi:10.5194/os-11-67-2015.

- Abraham, J. P., et al. (2013), A review of global ocean temperature observations: Implications for ocean heat content estimates and climate change, *Rev. Geophys.*, *51*, 450–483, doi:10.1002/rog.20022.
- Balmaseda, M. A., K. E. Trenberth, and E. Källén (2013), Distinctive climate signals in reanalysis of global ocean heat content, *Geophys. Res. Lett.*, *40*, 1754–1759, doi:10.1002/grl.50382.
- Cazenave, A., H.-B. Dieng, B. Meyssignac, K. von Schuckmann, B. Decharme, and E. Berthier (2014), The rate of sea-level rise, *Nat. Clim. Change*, doi:10.1038/nclimate2159.
- Chambers, D. P., and J. A. Bonin (2012), Evaluation of release-05 GRACE time-variable gravity coefficients over the ocean, *Ocean Sci.*, *8*, 859–868.
- Chen, X., and K.-K. Tung (2014), Varying planetary heat sink led to global-warming slowdown and acceleration, *Science*, *345*, 897–903.
- Cheng, M., and B. D. Tapley (2004), Variations in the Earth's oblateness during the past 28 years, *J. Geophys. Res.*, *109*, B09402, doi:10.1029/2004JB003028.
- Church, J. A., and N. J. White (2011), Sea-level rise from the late 19th to the early 21st century, *Surv. Geophys.*, *32*, 585–602.
- Dee, D. P., et al. (2011), The ERA-Interim reanalysis: Configuration and performance of the data assimilation system, *Q. J. R. Meteorol. Soc.*, *137*, 553–597.
- Desbruyères, D. G., S. Purkey, E. L. McDonagh, G. C. Johnson, and B. A. King (2016), Deep and abyssal ocean warming from 35 years of repeat hydrography, *Geophys. Res. Lett.*, *43*, 10,356–10,365, doi:10.1002/2016GL070413.
- Dieng, H. B., H. Palanisamy, A. Cazenave, B. Meyssignac, and K. von Schuckmann (2015), The sea level budget since 2003: Inference on the deep ocean heat content, *Surv. Geophys.*, *36*, 209–229, doi:10.1007/s10712-015-9314-6.
- Geruo, A., J. Wahr, and S. Zong (2013), Computations of the viscoelastic response of a 3-D compressible Earth to surface loading: An application of glacial isostatic adjustment in Antarctica and Canada, *Geophys. J. Int.*, *192*, 557–572, doi:10.1093/gji/ggs030.
- Hansen, J., M. Sato, P. Kharecha, and K. von Schuckmann (2011), Earth's energy imbalance and implications, *Atmos. Chem. Phys.*, *11*, 13,421–13,449.
- Hosoda, S., T. Ohira, and T. Nakamura (2008), A monthly mean dataset of global oceanic temperature and salinity derived from Argo float observations, *JAMSTEC Rep. Res. Dev.*, *8*, 47–59.
- IPCC (2013), *Climate Change 2013: The Physical Science Basis*, edited by T. F. Stocker et al., Cambridge Univ. Press, Cambridge, U. K.
- Jayne, S. R., J. M. Wahr, and F. O. Bryan (2003), Observing ocean heat content using satellite gravity and altimetry, *J. Geophys. Res.*, *108*(C2), 3031, doi:10.1029/2002JC001619.
- Johnson, G. C., and D. P. Chambers (2013), Ocean bottom pressure seasonal cycles and decadal trends from GRACE Release-05: Ocean circulation implications, *J. Geophys. Res. Oceans*, *118*, 4228–4240, doi:10.1002/jgrc.20307.
- Johnson, G. C., and J. M. Lyman (2014), Oceanography: Where's the heat?, *Nat. Clim. Change*, *4*, 956–957, doi:10.1038/nclimate2409.
- Johnson, G. C., J. M. Lyman, and S. G. Purkey (2015), Informing Deep-Argo array design using Argo and full-depth hydrographic section data, *J. Atmos. Oceanic Technol.*, *32*, 2187–2198, doi:10.1175/JTECH-D-15-0139.1.
- Kanamitsu, M., W. Ebisuzaki, J. Woollen, S.-K. Yang, J. J. Hnilo, M. Fiorino, and G. L. Potter (2002), NCEP-DOE AMIP-II Reanalysis (R-2), *Bull. Am. Meteorol. Soc.*, *83*, 1631–1643, doi:10.1175/BAMS-83-11-1631.
- Le Traon, P.-Y., F. Nadal, and N. Ducet (1998), An improved mapping method of multisatellite altimeter data, *J. Atmos. Oceanic Technol.*, *15*, 522–534, doi:10.1175/1520-0426(1998).
- Lee, S.-K., W. Park, M. O. Baringer, A. L. Gordon, B. Huber, and Y. Liu (2015), Pacific origin of the abrupt increase in Indian Ocean heat content during the warming hiatus, *Nat. Geosci.*, *8*, 445–450.
- Levitus, S., J. Antonov, and T. Boyer (2005), Warming of the world ocean, 1955–2003, *Geophys. Res. Lett.*, *32*, L02604, doi:10.1029/2004GL021592.
- Llovel, W., and T. Lee (2015), Importance and origin of halosteric contribution to sea level change in the southeast Indian Ocean during 2005–2013, *Geophys. Res. Lett.*, *42*, 1148–1157, doi:10.1002/2014GL062611.
- Llovel, W., J. K. Willis, F. W. Landerer, and I. Fukumori (2014), Deep-ocean contribution to sea level and energy budget not detectable over the past decade, *Nat. Clim. Change*, *4*, 1031–1035, doi:10.1038/nclimate2387.
- Loeb, N. G., J. M. Lyman, G. C. Johnson, R. P. Allan, D. R. Doelling, T. Wong, B. J. Soden, and G. L. Stephens (2012), Observed changes in top-of-the-atmosphere radiation and upper-ocean heating consistent within uncertainty, *Nat. Geosci.*, *5*, 110–113, doi:10.1038/ngeo1375.
- Masuda, S., et al. (2010), Simulated rapid warming of abyssal North Pacific waters, *Science*, *329*, 319–322, doi:10.1126/science.1188703.
- Mazloff, M. R., and C. Boening (2016), Rapid variability of Antarctic Bottom Water transport into the Pacific Ocean inferred from GRACE, *Geophys. Res. Lett.*, *43*, 3822–3829, doi:10.1002/2016GL068474.
- Menemenlis, D., J.-M. Campin, P. Heimbach, C. Hill, T. Lee, A. Nguyen, M. Schodlok, and H. Zhang (2008), ECCO2: High-resolution global ocean and sea ice data synthesis, *Mercat. Ocean Q. NewsL.*, *31*, 13–21.
- Peltier, W. R. (2004), Global glacial isostasy and the surface of the ice-age Earth: The ICE-5G(VM2) model and GRACE, *Annu. Rev. Earth Planet. Sci.*, *32*, 111–149.
- Purkey, S. G., and G. C. Johnson (2010), Warming of global abyssal and deep Southern Ocean waters between the 1990s and 2000s: Contributions to global heat and sea level budgets, *J. Clim.*, *23*, 6336–6351, doi:10.1175/2010JCLI3682.1.
- Purkey, S. G., and G. C. Johnson (2012), Global contraction of Antarctic Bottom Water between the 1980s and 2000s, *J. Clim.*, *25*, 5830–5844, doi:10.1175/JCLI-D-11-00612.1.
- Purkey, S. G., and G. C. Johnson (2013), Antarctic bottom water warming and freshening: Contributions to sea level rise, ocean freshwater budgets, and global heat gain, *J. Clim.*, *26*, 6105–6122, doi:10.1175/JCLI-D-12-00834.1.
- Purkey, S. G., G. C. Johnson, and D. P. Chambers (2014), Relative contributions of ocean mass and deep steric changes to sea level rise between 1993 and 2013, *J. Geophys. Res. Oceans*, *119*, 7509–7522, doi:10.1002/2014JC010180.
- Rienecker, M. M., et al. (2011), MERRA: NASA's Modern-Era Retrospective Analysis for Research and Applications, *J. Clim.*, *24*, 3624–3648, doi:10.1175/JCLI-D-11-00015.1.
- Roemmich, D., and J. Gilson (2009), The 2004–2008 mean and annual cycle of temperature, salinity, and steric height in the global ocean from the Argo Program, *Prog. Oceanogr.*, *82*, 81–100.
- Roemmich, D., J. Church, J. Gilson, D. Monselesan, P. Sutton, and S. Wijffels (2015), Unabated planetary warming and its ocean structure since 2006, *Nat. Clim. Change*, *5*, 240–245, doi:10.1038/nclimate2513.
- Roemmich, D., J. Gilson, P. Sutton, and N. Zilberman (2016), Multidecadal change of the South Pacific gyre circulation, *J. Phys. Oceanogr.*, *46*, 1871–1883, doi:10.1175/JPO-D-15-0237.1.
- Swenson, S., D. Chambers, and J. Wahr (2007), Estimating geocenter variations from a combination of GRACE and ocean model output, *J. Geophys. Res.*, *113*, B08410, doi:10.1029/2007JB005338.
- Tamisiea, M. E., and J. X. Mitrovica (2011), The moving boundaries of sea level change: Understanding the origins of geographic variability, *Oceanography*, *24*(2), 24–39, doi:10.5670/oceanog.2011.25.
- Trenberth, K. E., and J. T. Fasullo (2010), Tracking Earth's energy, *Science*, *328*, 316–317.

- Volkov, D.L., S.-K. Lee, R. Lumpkin (2015), On the mechanisms of deep-ocean warming in the South Pacific, paper presented at NASA Ocean Surface Topography Science Team meeting, Reston Va., Oct. 20–23. [Available at http://meetings.aviso.altimetry.fr/fileadmin/user_upload/tx_ausycisseminar/files/Poster1_OSTST_Oct2015.pdf.]
- Von Schuckmann, K., et al. (2016), An imperative to monitor Earth's energy imbalance, *Nat. Clim. Change*, 6, 138–144, doi:10.1038/nclimate2876.
- Wahr, J., R. S. Nerem, and S. V. Bettadpur (2015), The pole tide and its effect on GRACE time-variable gravity measurements: Implications for estimates of surface mass variations, *J. Geophys. Res. Solid Earth*, 120, 4597–4615, doi:10.1002/2015JB011986.
- Willis, J. K., D. P. Chambers, and R. S. Nerem (2008), Assessing the globally averaged sea level budget on seasonal to interannual time scales, *J. Geophys. Res.*, 113, C06015, doi:10.1029/2007JC004517.